Determining mass limits around HD163296 through SPHERE direct imaging data

Journal Article

Author(s):
Mesa, Dino; Langlois, Maud; Garufi, Antonio; Gratton, Raffaele; Desidera, Silvano; D'Orazi, Valentina; Flasseur, Olivier; Barbieri, Mauro; Benisty, Myriam; Henning, Thomas; Ligi, R.; Sissa, Elena; Vigan, Arthur; Zurlo, Alice; Boccaletti, Anthony; Bonnefoy, Mickaël; Cantalloube, Faustine; Chauvin, Gaël; Cheetham, Anthony; De Caprio, Vincenzo; Delorme, Philippe; Feldt, Markus; Fusco, T.; Gluck, L.; Hagelberg, Janis ⓘD; Lagrange, Anne-Marie; Lazzoni, Cecilia; Madec, F.; Maire, A.-L.; Ménard, F.; Ramos, J.; Rickman, E.L.; Rouan, Daniel; Schmidt, T.; van der Plas, Gerrit

Determining mass limits around HD 163296 through SPHERE direct imaging data

D. Mesa,[1,2]* M. Langlois,[3,4] A. Garufi,[5] R. Gratton,[1] S. Desidera,[1] V. D'Orazi,[1]
O. Flasseur,[6] M. Barbieri,[2] M. Benisty,[7,8] T. Henning,[9] R. Ligi,[10] E. Sissa,[1] A. Vigan,[4]
A. Zurlo,[4,11,12] A. Boccaletti,[13] M. Bonnefoy,[7] F. Cantalloube,[8] G. Chauvin,[7]
A. Cheetham,[14] V. De Caprio,[15] P. Delorme,[8] M. Feldt,[9] T. Fusco,[4,16] L. Gluck,[8]
J. Hagelberg ●,[17] A.-M. Lagrange,[8] C. Lazzoni,[1] F. Madec,[4] A.-L. Maire,[9,18]
F. Menard,[8] M. Meyer,[17,19] J. Ramos,[9] E.L. Rickman,[14] D. Rouan,[13] T. Schmidt[13,20] and
G. Van der Plas ●[7]

Affiliations are listed at the end of the paper

ABSTRACT

HD 163296 is a Herbig Ae/Be star known to host a protoplanetary disc with a ringed structure. To explain the disc features, previous works proposed the presence of planets embedded into the disc. We have observed HD 163296 with the near-infrared (NIR) branch of SPHERE composed by IRDIS (InfraRed Dual-band Imager and Spectrograph) and IFS (integral field spectrograph) with the aim to put tight constraints on the presence of substellar companions around this star. Despite the low rotation of the field of view during our observation we were able to put upper mass limits of few M_{Jup} around this object. These limits do not allow to give any definitive conclusion about the planets proposed through the disc characteristics. On the other hand, our results seem to exclude the presence of the only candidate proposed until now using direct imaging in the NIR even if some caution has to be taken considered the different wavelength bands of the two observations.

Key words: instrumentation: spectrographs – methods: data analysis – techniques: imaging spectroscopy – (stars:) planetary systems, HD 163296.

1 INTRODUCTION

The most promising environments to search for in-formation planetary systems are protoplanetary discs around very young stars (see e.g. Chen et al. 2012; Marshall et al. 2014). These systems can be probed both with high-contrast imaging in the near-infrared (NIR) through instruments like SPHERE (Beuzit et al. 2019), GPI (Macintosh et al. 2014), Keck/NIRC2 (Mawet et al. 2017), and CHARIS at Subaru Telescope (Groff et al. 2015) and at submillimetre wavelengths with instruments like ALMA. One noteworthy example of the first case is the recently discovered planet around the disc hosting star PDS 70 (Keppler et al. 2018; Müller et al. 2018). On the other hand, in recent years an increasing number of protoplanetary disc with gaps and rings have been imaged through ALMA (e.g. ALMA Partnership et al. 2015; Andrews et al. 2016;

Loomis et al. 2017; Ansdell et al. 2018; Fedele et al. 2018; Huang et al. 2018; Pinilla et al. 2018). One of the most promising model to explain these structures implies that they are due to the interactions between the disc and planetary mass objects (e.g. Bryden et al. 1999; Jin et al. 2016). However, plenty of alternative models have been proposed to explain these structures including dust accumulations at the snowlines (e.g. Zhang, Blake & Bergin 2015), zonal flows (e.g. Béthune, Lesur & Ferreira 2017), or secular gravitational instability (e.g. Takahashi & Inutsuka 2014). Clearly, having the possibility to directly image the foreseen planetary companions into these discs or, alternatively, to put tight limits on the masses of these objects could help to disentangle between the proposed models.

HD 163296 (HIP 87819) is an A1V spectral-type (Mora et al. 2001) Herbig Ae/Be star at a distance of 101.5 ± 1.2 pc from the Sun (Gaia Collaboration et al. 2018). Recently, its stellar parameters were defined by Setterholm et al. (2018) fitting its *H*- and *K*-band flux with the *PARSEC* models (Bressan et al. 2012) and finding an age of 10.4 Myr and a mass of 1.9 $M_\odot$. We will assume these

parameters in this work. It is important, however, to note that there is a discrepancy between the age we are assuming and the evolutionary stage of the disc around this star as deduced by the observations (see below). From this point of view, the previous age determination around 4–5 Myr (e.g. van den Ancker, de Winter & Tjin A Djie 1998; Montesinos et al. 2009) would be in a better agreement with the disc evolutionary stage. In any case, with an estimated T_{eff} of ∼9200 K, we would need a luminosity about two times the predicted 16 $L_{\odot}$ to be able to fit the evolutive track of a 4–5 Myr star. In addition, the previous determinations of the age of the star were obtained assuming a distance of ∼122 pc and not the more recent value given above.

The presence of dust associated with this star was first demonstrated through observations at millimeter wavelengths (see e.g. Mannings & Sargent 1997). Observations in the infrared (IR) proved the presence of warm gas and silicate in the disc (e.g. Sitko et al. 1999), while observations in the visible allowed Grady et al. (2000) to define a radius as ∼500 au. The mass of the disc was estimated between 0.01 and 0.15 $M_{\odot}$ (Isella et al. 2007; Tilling et al. 2012). A first detection of the presence of a ring structure in this disc was obtained by Garufi et al. (2014, 2017) using polarized NIR data taken with NACO at the VLT.

More recently, Isella et al. (2016) revealed, using ALMA data taken with a resolution of 20 au, the presence of three dark concentric gaps at 45, 87, and 140 au and of three bright rings at 68, 100, and 160 au from the star. Like for other works on this target, they used a distance of 122 pc for the system (van den Ancker et al. 1997) instead of the more recent value cited above. Here and for all the works that used the old distance that are cited in this paper, we have then updated the value of the separations using the updated value of the distance. To explain the ring structure, they proposed that the two external gaps were due to the presence of two planets, both of them with a mass of ∼0.3 M_{Jup}. On the other hand, they were not able to explain the inner gap with the presence of a single planet. It has to be explained by a different physical process or by the presence of more than one planet with a Saturn-like mass. However, using the same data and comparing them with 2D-hydrodynamic simulations, Liu et al. (2018) were able to explain all of the gaps with the presence of planets with masses of 0.46, 0.46, and 0.58 M_{Jup} at a separation of 48, 86, and 131 au, respectively. To reach this goal, they have to assume a disc with a viscosity variable from less than 10^{-4} in the inner disc to ∼7.5 × 10^{-3} in the outer disc. On the other hand, van der Marel, Williams & Bruderer (2018) demonstrated that it is possible to explain the gaps through models with grain growth at radii corresponding to the snowlines of molecules like e.g. CH_4 and CO. Afterwards, the presence of two planets was proposed by Teague et al. (2018) through a new method to measure the rotation curve of the CO into the disc that allowed to determine substantial deviations from the Keplerian velocity. The two proposed planets are at a separation of 83 and 137 au from the central star and have a mass of 1 and 1.3 M_{Jup}, respectively. A further planetary mass companion was proposed by Pinte et al. (2018) that found a localized deviation from the Keplerian velocity of the molecular gas in the protoplanetary disc. In this latter case, they were also able to propose not only a separation for the planet but also its approximate position. Indeed, the proposed planet has a separation of 2.3 ± 0.2 arcsec (corresponding to a distance of around 260 au) from the central star and a position angle of −3° ± 5°. The mass of this object should be ∼2 M_{Jup}. Finally, Dong et al. (2018) proposed, using two-fluid hydrodynamic simulations, that a single planet with a mass of 65 $M_{\oplus}$ at a separation of 108 au

can account for the ring structure of the disc if it has a very low viscosity (less than 10^{-4}).

HD 163296 was also observed in the NIR with GPI (Monnier et al. 2017) in *J*-band polarized light, with SPHERE using the polarized mode of IRDIS (Langlois et al. 2014) in both *J* and *H* bands (Muro-Arena, Dominik & Waters 2018) and with HiCIAO and CHARIS at Subaru both in polarized light and high-contrast spectroscopy (Rich et al. 2019). In all these cases, they were able to observe only the ring at ∼67 au from the star.

The star was also observed in high-contrast imaging with Keck/NIRC2 by Guidi et al. (2018) in L' spectral band. They were able to put a mass limit of 8–15 M_{Jup}, 4.5–6.5 M_{Jup}, and 2.5–4 M_{Jup} at the position of the three gaps detected by Isella et al. (2016). Furthermore, they identified a point source at ∼0.5 arcsec and at a position angle of ∼30°. This would correspond to a distance of 67 au from the star near the inner edge of the second gap in the disc, while they proposed for this object a mass of ∼6 M_{Jup}. Regarding the disc, also in this case only the inner bright ring of the disc was partially imaged.

Finally, a new ALMA observation in the context of the DSHARP (Andrews et al. 2018) project was taken at a resolution of ∼4 au by Isella et al. (2018). This allowed to confirm the ring structure found in the previous observation. Moreover, a new gap-bright ring combination was identified at ∼10 au from the star together with a substructure in the first ring.

The large disc mass together with the relatively old stellar age is a further hint of the presence of embedded planets, as it supports the existence of dust traps generated by the presence of companions preventing the accretion of material on the star for a long time-scale (Garufi et al. 2018).

We have used SPHERE to observe HD 163296 in high-contrast imaging with the aim to disentangle between the proposed models explaining its disc structure and to put limits on the masses of substellar objects around this star. In this paper, we give the results obtained from these observations that were obtained in the context of the SHINE (SPHERE High-contrast imaging survey for Exoplanets) survey (Chauvin et al. 2017). In Section 2, we present the data set and detail the data reduction method, while in Section 3, we display the results. Finally, in Section 4 we discuss them and give the conclusions.

2 OBSERVATIONS AND DATA REDUCTION

HD 163296 was observed during the nights of 2017-09-29 and 2018-05-06 with SPHERE operating in the IRDIFS_EXT mode. In this mode, InfraRed Dual-band Imager and Spectrograph (IRDIS; Dohlen et al. 2008) operates in dual-band imaging (Vigan et al. 2010) configuration with the *K*1–*K*2 filters (*K*1 = 2.110 µm; *K*2 = 2.251 µm), while integral field spectrograph (IFS; Claudi et al. 2008) works in the *Y*–*H* spectral bands between 0.95 and 1.65 µm. In the first epoch, the total exposure time was of 1536 s with IRDIS and of 1728 s with IFS, while in the second epoch, it was of 4608 s with both instruments. The weather conditions of the two epochs are detailed in Table 1 and were generally good. However, the main limitation to the contrast that can be obtained from these observations is the low rotation of the field of view (FOV) especially for what concerns the first epoch, as can be seen in Table 1. This is due to the fact that the declination of HD 163296 is very near to the Paranal Observatory latitude preventing from observing it during the passage of the star at meridian because of VLT pointing

Table 1. Characteristics of the SPHERE observations of HD 163296. In column 2, we list the observing mode used (see the text for more details) and in column 3 we report the coronagraph used. In columns 4 and 5, we list the number of datacubes, the number of frames for each datacube, and the exposure time, given in s, for each frame for the IRDIS and IFS data, respectively. In column 6, we list the total rotation of the FOV during the observation, while in columns 7, 8, and 9, we report the median values of seeing, coherence time, and wind speed during the observations.

Date	Obs. mode	Coronagraph	Obs. IRDIS	OBs IFS	RA (deg)	S (arcsec)	τ_0 (ms)	wind (m s^{-1})
2017-09-29	IRDIFS_EXT	N_ALC_YJH_S	4 × 12;32	18 × 12;8	1.33	0.68	5.4	3.38
2018-05-06	IRDIFS_EXT	N_ALC_Ks	9 × 16;32	3 × 16;96	16.02	0.67	3.7	9.07

restrictions at less than 3° from the zenith. This is a severe limit to the total rotation of the FOV.

Both IRDIS and IFS data were reduced using the SPHERE data reduction and handling (DRH; Pavlov et al. 2008) pipeline, exploiting the SPHERE data centre (Delorme et al. 2017) interface. We also used, to implement the speckle subtraction procedures, the SpeCal tool (Galicher et al. 2018) appositely developed for SPHERE data reduction. IFS data reduction was performed using the procedure described by Zurlo et al. (2014) and Mesa et al. (2015) to create calibrated datacubes composed of 39 frames at different wavelengths on which we applied the principal components analysis (PCA; e.g. Soummer, Pueyo & Larkin 2012; Amara, Quanz & Akeret 2015) to reduce the speckle noise. This algorithm allowed us to implement at the same time both angular differential imaging (ADI; Marois et al. 2006) and spectral differential imaging (SDI; Racine et al. 1999). The self-subtraction was appropriately taken into account by injecting in the data fake planets at different separations. IRDIS data were reduced following the procedure described by Zurlo et al. (2016) and applying the PCA algorithm for the reduction of the speckle noise. For all the data set, the contrast was calculated following the procedure described by Mesa et al. (2015) taking into account the small sample statistics as devised in Mawet et al. (2014). Despite the limitations of the adopted method, showed by recent works (Ruane et al. 2017; Jensen-Clem et al. 2018), we found that the approach that we adopted is able to provide reliable limits for the present case.

An alternative data reduction has been performed using PACO (Flasseur et al. 2018) for IRDIS and PACO-ASDI (Flasseur et al., in preparation) for IFS. Contrary to existing approaches, this method models the background statistics to locally capture the spatial (PACO) and spectral (PACO-ASDI) correlations at the scale of a patch of a few tens of pixels. Since PACO locally learns the background fluctuations, the aberrant data or the larger stellar leakages can also be learned locally as typical background fluctuations and are not interpreted in the detection stage as the signature of an exoplanet. The method produces both stationary and statistically grounded detection maps, as well as the false alarm rate and the probability of detection, that have been proven to be robust by fake planet injections. The detection maps are robust to defective pixels and other aberrant data points arising during the SPHERE observations or data pre-processing pipeline. The patches considered in the PACO algorithm define the characteristic size of the areas in which the statistics of the background fluctuations are modelled. Their size obeys a trade-off: on the one hand, the larger the patches, the more energy from the source is contained in the patches that improves the signal-to-noise ratio; on the other hand, learning the covariance of larger patches requires more temporal diversity. In practice, since the sources to be detected are faint compared to the level of stellar speckles and their temporal fluctuations, the optimal patch size corresponding to twice the off-axis PSF full width at half-maximum (FWHM) is used (leading to patch radii of 4 and 5 pixels for K1 and K2 filters, respectively) to produce the contrast limits (Fig. 3). However, given that this method is new, we will
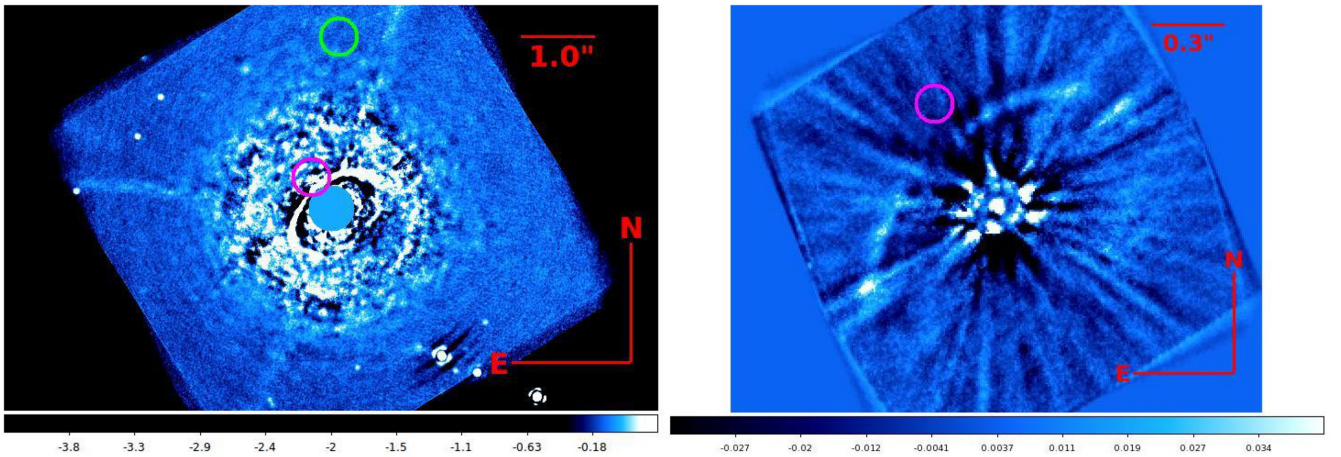

Figure 1. Final images obtained from the 2018-05-06 observations. In both cases, the values are expressed in counts. *Left:* IRDIS final image obtained applying the PCA algorithm and subtracting 1 mode from the original data. The green circle is to enlight the zone around the planet proposed by Pinte et al. (2018), the magenta circle enlight the zone of the planet proposed by Guidi et al. (2018). The mask covering the star has a radius of 0.37 arcsec. *Right:* IFS final image obtained using the PCA algorithm subtracting 1 mode from the original data. As for the IRDIS image, the magenta circle identify the zone around the planet proposed by Guidi et al. (2018).
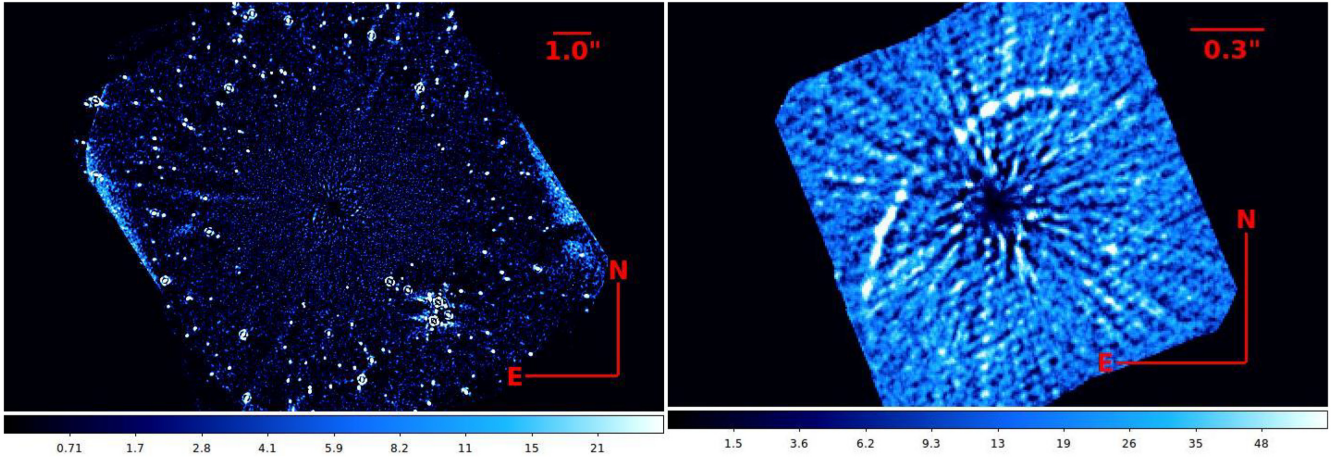
Figure 2. GLR maps obtained using PACO from the 2018-05-06 observations. In the left-hand panel, we display the IRDIS image, while in the right-hand panel, we display the IFS image.

use in the following the PACO contrast values as a lower limit while the PCA contrast will be used as conservative values for the contrast.

3 RESULTS

In Fig. 1, we display the final images that we obtain from the IRDIS (left-hand panel) and IFS (right-hand panel) data using the PCA-based data reduction, while in Fig. 2, we display the generalized likelihood ratio (GLR; Flasseur et al. 2018) map obtained from PACO and PACO-ASDI for IRDIS and IFS, respectively. Within the PACO framework, GLR is defined by GLR $= \sum_{\lambda=1}^{L} \max(\mathrm{SNR}_\lambda, 0)^2$. While it is not statistically grounded when $L \neq 1$ (as is the case for the IFS image), it is used here as a simple combination of the available spectral channels to emphasize structures at weak level of contrast.

3.1 Disc detection

Like for previous NIR observations, we are able to detect only the first ring of the disc. As pointed out by Muro-Arena et al. (2018), this is probably due to the lack of small dust grain on the surface of the outer disc.

The signal-to-noise ratio (SNR) of the detection is however low both with IRDIS (with a value of ∼7.5 in the brightest part of the disc and median values below 3) and IFS (with values around or below 2) and, in particular in the IFS case, it appears incomplete. Despite this is not the main goal of our observations, we derived the main parameters of the disc following a procedure similar to that devised in Gibbs et al. (2019) using the model Zodipic (Kuchner 2012). This procedure is aimed to maximize the cross-correlation between synthetic discs obtained using the Zodipic model with different parameters and our data. To this aim, we used the second epoch IRDIS data that allowed the best imaging of the disc between our data. At the end of this procedure, we found for the bright ring an inclination of 49.3° ± 2.0°, a position angle of 133.6° ± 2.0° and radius of ∼63 ± 3 au. The values of the offset were of −16.6 ± 10.0 mas in *X* and of −0.5 ± 10.0 mas in *Y*. These values are similar to those obtained from previous work aimed to study the disc (e.g. Isella et al. 2018; Muro-Arena et al. 2018), but of course the results are plagued by the low SNR obtained for the disc from our data.
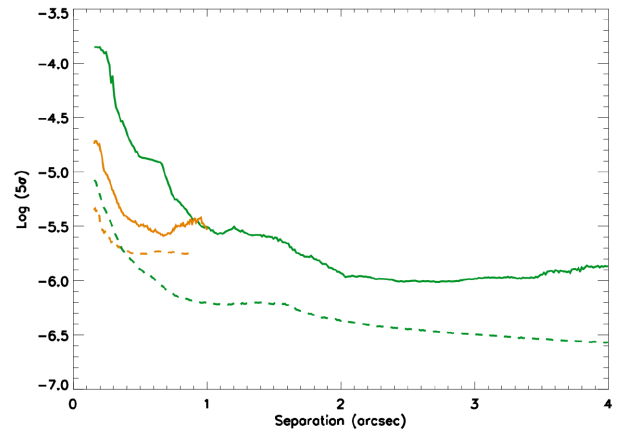

Figure 3. 5σ contrast versus separation expressed in arcsec obtained for IRDIS (solid green line) and for IFS (solid orange line) using the PCA algorithm and subtracting 1 mode from the original data as done for the images shown in Fig. 1. The dashed lines represent the contrast obtained using PACO using patch radii of 4 and 5 pixels for *K*1 and *K*2 filters, respectively.

3.2 Detection limits

Deep high-contrast imaging data allow to put much tighter constraints on the mass of possible substellar companion around HD 163296 than the polarized data. In Fig. 3, we display the contrast versus the separation both for IRDIS (green line) and IFS (orange line) using the data from the second epoch, when we were able to obtain a deeper contrast, applying the PCA algorithm. We also display, using dashed lines of the same colours of the PCA plots, the contrast obtained using the PACO algorithm both for IRDIS and IFS. To take into account the inclination of the disc, we have deprojected the separations on our images adopting an inclination of 46.7° and a position angle of 133.3° as found by Isella et al. (2018). Despite the low rotation of the FOV, we are able to obtain a contrast better than 10^{-5} at separations of few tenths of arcsec with IFS, while IRDIS allows to obtain a contrast of the order of 10^{-6} at separation larger than 2 arcsec. PACO allows to obtain a gain of around three times for the IRDIS case, while the gain is less important in the IFS case.
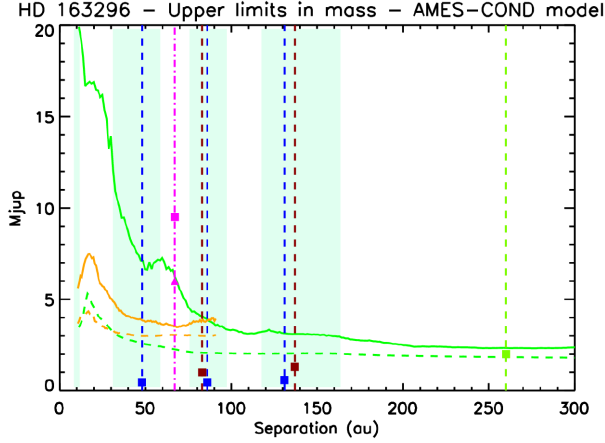
Figure 4. Mass limits versus the separation from the central star expressed in au for IRDIS (green line) and for IFS (orange line) obtained using the AMES-COND models. The dashed lines in the same colours represents the mass limits obtained using PACO. The light cyan areas represent the estimated positions of the gaps around the star as estimated in Isella et al. (2018). We also overplot the dashed lines that represent the positions of the planets proposed by Liu et al. (2018) (blue lines), Teague et al. (2018) (red lines), Pinte et al. (2018) (green line) and Guidi et al. (2018) (magenta line). Further, we added the foreseen mass of each proposed planet denoting them with a filled square of the same colour of the corresponding line. In the case of the planet proposed by Guidi et al. (2018) we used a filled triangle to show the mass of the planet as proposed in the paper and the updated value of planetary mass with a filled square (see the text for more details).

For what concerns the planets proposed in previous works to explain the disc structure, in Fig. 1 we have highlighted, both in IRDIS and IFS image, with a magenta circle the region around the position of the 6 M_{Jup} planet proposed by Guidi et al. (2018) through direct imaging. In both cases, we are not able to find any evidence of the proposed companion. Moreover, in the IRDIS image we also display a green circle to enlight the region around the 2 M_{Jup} planet proposed by Pinte et al. (2018). Also in this case, the proposed planet is not visible in our data.

Using the contrast values obtained with the procedure described above and the AMES-COND (Allard et al. 2003) and the AMES-DUSTY (Allard et al. 2001) evolutionary models, we calculated the mass limits for substellar objects around HD 163296. The choice of these models gives the possibility to explore different and extreme conditions that are absolute absence of clouds in the first case and complete clouds coverage in the latter case. To this aim, we assumed for the system the age and the distance given in Section 1. Moreover, we assumed for the star a magnitude H of 5.53 and a magnitude K of 4.78 (Cutri et al. 2003). The results of this procedure are displayed in Figs 4 and 5, where the orange lines represent the limits obtained through IFS and the green lines represent the limits obtained through IRDIS. As for Fig. 3, we display with dashed lines the mass limits obtained using the contrast from PACO. With PCA, IFS allows, at separations between 30 and 80 au, to exclude the presence of substellar objects with mass larger than 3–4 M_{Jup} if we consider the AMES-COND models, while the AMES-DUSTY models imply a larger limit between 6 and 7 M_{Jup}. At larger separations, IRDIS allows to put limits of the order of 3–4 M_{Jup} up to ∼200 au and lower than 3 M_{Jup} at larger separations when considering the AMES-COND models, while the limits with the AMES-DUSTY models are of 4–5 M_{Jup} at the same separations. PACO allows to improve especially at short
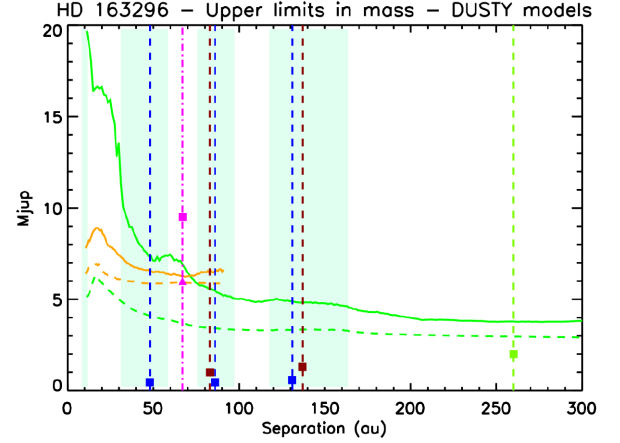

Figure 5. Same than Fig. 4 but for mass limits obtained using DUSTY models.

Table 2. Mass limits expressed in M_{Jup} at the estimated positions of the gaps in the disc of HD 163296 calculated both with AMES-COND (third column) and AMES-DUSTY (fourth column) models. In both cases the limit are expressed in M_{Jup}. In the second column we report the separation expressed in au of each gap as found by Isella et al. (2018).

Gap	Separation	A.-C. M. lim.	A.-D. M. lim.
1	45	3.7–4.9	6.4–7.3
2	87	3.4–4.5	5.0–6.6
3	159	3.0–3.3	4.6–5.0

separations while at larger separations the IRDIS mass limits tends to converge to similar values obtained with the PCA method. In the same images, we coloured in light cyan the zones of the gaps defined by Isella et al. (2018) and we overplotted dashed vertical lines at the separations foreseen for the planets proposed by Liu et al. (2018), Teague et al. (2018), Pinte et al. (2018), and Guidi et al. (2018), adding also a filled square indicating the mass of each proposed planet. We can use these results to put limits at the gaps positions. The inner one, recently discovered lay behind the SPHERE coronagraph so that we cannot put any constraints about it. The calculated limits for the other three gaps with both the adopted models are listed in Table 2 and are of the order of a few M_{Jup}.

It is clear, however, that the depth of our observations is not enough to detect the planets proposed both by Liu et al. (2018) and Teague et al. (2018) both considering the limits with AMES-COND and AMES-DUSTY models. On the other hand, the planet of 6 M_{Jup} at a projected separation of ∼67 au as proposed by Guidi et al. (2018) should be visible with IFS while it should be at the detection limit with IRDIS (filled triangle in Fig. 4) with AMES-COND models while it should be below the detection limits with the AMES-DUSTY models. It has to be noted, however, that the mass of 6 M_{Jup} was obtained assuming an age of 5 Myr obtained from Montesinos et al. (2009). If we reconsider the mass of this companion using the age used in this work, it would have a mass between 9 and 10 M_{Jup} well above the detection limits with both the instruments and with both the adopted models. As written above, we are not able to detect this object in the final images obtained both with IFS and IRDIS as enlighted in the magenta circle displayed in Fig. 1. To exist without being detected in our data, this objects should be very red with a $H - L \sim 4.6$ and a $K - L \sim 2.5$. Finally,
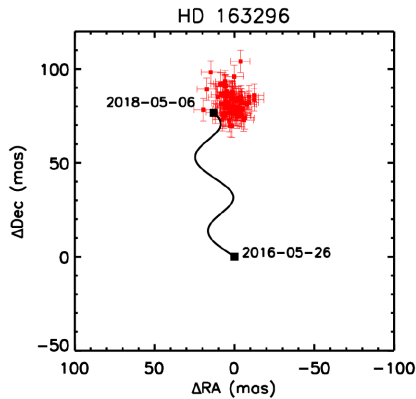
Figure 6. Differential motion in right ascension and in declination of the cross-identified sources between the SPHERE polarized data and the last observing data represented by the red squares. The black line represents the stellar motion due to proper motion and to annual parallax. The dark squares indicate the differential positions, relative to the first epoch, that a background object would have.

Figure 7. *K*1 versus *K*1–*K*2 colour–magnitude diagram with the positions of the candidates detected in the HD 163296 IRDIS FOV for which it was not possible to apply the proper motion test. These objects are represented by red and green asterisks while squares and diamond with different colours represent field dwarfs with spectral types as indicated in the plot legend. Large part of these objects (red asterisks) are in a position of the diagram that confirm they are background objects. Three of them (green asterisks) are in a positions that does not allow a definitive conclusion about them.

the planet proposed by Pinte et al. (2018) should be just below the detection limit of the IRDIS data using the AMES-COND models while it is well below the detection limits using the AMES-DUSTY models. Probably, given the disc environment rich of gas and dust in which the proposed planet is located the latter would be the more adequate in this case and this might explain why we are not able to detect it.

3.3 Candidate companions

Not surprisingly, given that the star is in the direction of the galactic center, the IRDIS FOV contains a lot of point-like sources. We have identified 111 of them in the first epoch and 166 in the second one when we were able to get much deeper images. We were able to cross-identify 91 of them between the two epochs. The objects that were identified in the first epoch but not in the second one were all near to the edge of the IRDIS FOV in the first epoch so that they were outside in the second one. Given the short time-span between the two epochs that did not allow a good use of the proper motion test, we decided to use also SPHERE *H*-band polarized data taken in the night 2016-05-26 and used for the work in Muro-Arena et al. (2018). In this latter case, we identify 92 point-like sources and 82 of them were successfully cross-identified with sources in the last epoch. All these targets are background objects as demonstrated by the proper motion test displayed in Fig. 6. The remaining targets identified just in the last epoch are very low-luminosity sources at large (>3 arcsec) projected separation from HD 163296. With very high probability they also are background objects. To further confirm this we have plotted these objects in *K*1 versus *K*1–*K*2 colour–magnitude diagram comparing them with the positions of field dwarfs objects as displayed in Fig. 7. The positions of large part of them confirm that they actually are background objects. Just for three of them it is not possible to draw a definitive conclusion as they are in a part of the diagram compatible with the positions of companion objects. In Table 3, we list the separations in right ascension and in declination of the 166 point source identified in the second observing epoch together with the status of each object.
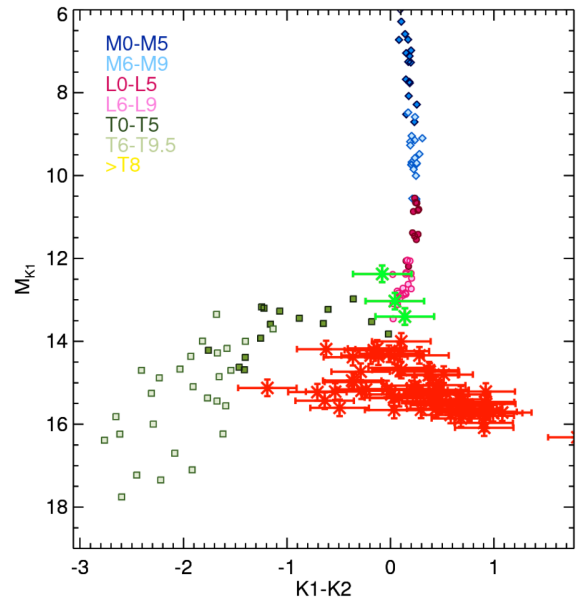
4 DISCUSSION AND CONCLUSIONS

In this work, we have presented the results of SPHERE SHINE observations of the Herbig star HD 163296. The effectiveness of these observations is mainly limited by the fact that it is not possible to observe this star during the passage through the meridian from Paranal Observatory. For this reason the total rotation of the FOV cannot be large during the observation limiting the contrast deepness that can be reached through high-contrast imaging techniques like ADI. Despite this limitation we were however able to obtain a contrast better than 10^{-5} at separation less than 1 arcsec thanks to IFS and of the order of 10^{-6} at separations larger than 2 arcsec thanks to IRDIS. This contrast allows to put mass limits between 3 and 4 M_{Jup} or 6 and 7 M_{Jup} at projected separations between 30 and 80 au using the AMES-COND and AMES-DUSTY models, respectively. Furthermore, IRDIS allows to obtain mass limit of $\sim$2 M_{Jup} or $\sim$4 M_{Jup} at projected separations larger than 200 au using AMES-COND and AMES-DUSTY, respectively. Given the environment around HD 163296, the latter is probably the more adequate to this case. The use of both models can however give an idea of the range of variability of the mass limit around this target. For this work, we have assumed an age of the system of 10.4 Myr obtained by a recent determination contrarily to what was generally done in the previous works on this object that used an older determination of the age (5 Myr). This of course results in higher mass limits that are however more reliable than those obtained using the younger age.

It is anyhow important to stress that these limits do not take into account the effects of the material (dust or gas) of the disc on the visibility of companions around HD 163296. Indeed, if they are embedded in the disc or behind it, we would expect that they are extremely reddened or suffering large amounts of extinction so

Table 3. List of point sources found in the HD 163296 IRDIS FOV at 2018-05-06 epoch. The second and third columns give the separation, expressed in mas, from the star in right ascension and in declination respectively. The status values in column 4 are: background object by proper motion test (1); background object by photometry (2); undefined (3).

Id.	$\Delta\alpha$	$\Delta\delta$	Status	Id.	$\Delta\alpha$	$\Delta\delta$	Status	Id.	$\Delta\alpha$	$\Delta\delta$	Status
1	− 509.00	5462.37	1	57	645.59	− 4879.25	1	113	− 5197.64	− 3883.85	2
2	− 410.41	4994.64	1	58	1662.26	3569.96	1	114	− 4215.46	− 3812.74	2
3	− 299.90	4538.29	1	59	1125.33	− 5559.30	1	115	− 3625.25	− 3451.66	2
4	− 985.98	4541.28	1	60	2319.59	− 5044.66	1	116	− 3690.08	− 4459.15	2
5	− 1676.50	4473.01	1	61	2410.89	− 3366.61	1	117	− 2612.69	− 4643.71	2
6	270.84	4874.09	1	62	3693.00	− 3210.14	1	118	− 2325.86	− 4715.11	2
7	1220.65	4940.52	1	63	1662.26	3569.96	1	119	− 2205.00	− 3466.75	2
8	2172.12	5120.92	1	64	3868.75	− 2409.64	1	120	− 805.54	− 3762.94	2
9	2360.17	5030.16	1	65	4402.96	− 2636.94	1	121	− 701.18	− 3606.38	2
10	2649.85	5399.47	1	66	4480.68	− 1945.64	1	122	− 1471.83	− 2469.98	2
11	2520.20	4418.24	1	67	5136.88	− 1493.52	1	123	− 467.72	− 3099.78	3
12	2658.56	4415.95	1	68	4771.12	− 160.86	1	124	− 538.31	− 4245.59	2
13	529.31	3161.66	1	69	4522.26	− 219.04	1	125	− 144.50	− 4187.11	2
14	1305.58	3548.11	1	70	3413.44	230.48	1	126	255.88	− 3992.68	2
15	1401.44	3603.88	1	71	3079.69	− 774.57	1	127	− 652.68	− 4778.69	2
16	1662.26	3569.96	1	72	3317.67	− 649.42	1	128	92.89	− 4730.31	2
17	1890.13	3473.17	1	73	4236.86	1020.44	1	129	1226.90	− 4587.38	2
18	1569.48	2933.20	1	74	4621.78	1055.75	1	130	742.31	− 4113.75	2
19	2793.61	3146.72	1	75	4740.98	1561.58	1	131	1171.58	− 5135.95	2
20	3075.84	2745.79	1	76	1662.26	3569.96	1	132	− 489.67	− 5879.36	2
21	2510.02	2004.26	1	77	3798.52	2093.64	1	133	553.83	− 5409.67	2
22	2283.82	1484.59	1	78	3973.68	2193.86	1	134	1454.72	− 5609.35	2
23	2594.07	958.99	1	79	3932.87	2310.46	1	135	2027.80	− 5762.07	2
24	− 2258.35	3155.69	1	80	4628.56	2877.03	1	136	2331.47	− 6007.90	2
25	− 2338.29	2645.61	1	81	5251.38	2754.56	1	137	2395.95	− 5752.67	3
26	− 2726.26	3378.10	1	82	3816.38	3990.23	1	138	2776.32	− 4259.94	2
27	− 3496.10	2949.37	1	83	− 417.92	4360.16	2	139	3249.41	− 4412.67	2
28	− 2881.48	1545.46	1	84	− 758.96	4997.35	2	140	3346.74	− 3616.26	2
29	− 4463.75	1710.53	1	85	− 1233.94	5038.10	2	141	3114.07	− 3905.03	2
30	− 4048.22	895.79	1	86	− 1408.75	5328.75	2	142	3899.05	− 3396.08	2
31	− 4209.64	219.15	1	87	− 1046.24	6113.48	2	143	3254.30	− 2404.37	2
32	− 4685.52	− 297.98	1	88	− 1696.50	5305.74	2	144	3960.09	− 1343.04	2
33	− 5384.59	− 1621.05	1	89	− 2028.89	5891.10	2	145	5163.41	589.75	2
34	− 3983.37	− 1187.56	1	90	− 2209.40	5105.29	2	146	6162.53	740.95	2
35	− 4434.98	− 1722.93	1	91	− 2148.81	3917.88	2	147	5124.51	1182.32	2
36	− 3357.80	− 2217.04	1	92	− 1880.89	3687.65	2	148	4756.92	1815.45	2
37	− 3020.95	− 2852.82	1	93	− 2309.81	6105.89	2	149	3445.42	1555.50	2
38	− 2751.01	− 2513.86	1	94	− 3102.85	5124.33	3	150	2903.25	2045.75	2
39	− 2636.81	− 3006.37	1	95	− 3202.02	4760.47	2	151	1531.25	2682.75	2
40	− 1947.87	− 2195.32	1	96	− 3035.23	4713.71	2	152	5546.39	3438.70	2
41	− 1663.77	− 2166.46	1	97	− 2986.02	4117.62	2	153	4825.14	3080.92	2
42	− 1473.32	− 1967.74	1	98	− 2717.43	3279.79	2	154	4062.91	3211.32	2
43	− 4067.00	− 3328.25	1	99	− 2603.90	2433.66	2	155	4124.00	3618.58	2
44	− 3056.33	− 3808.62	1	100	− 4020.27	2323.83	2	156	3337.48	4234.68	2
45	− 3490.52	− 4895.52	1	101	− 2778.04	1651.68	2	157	3728.81	4463.81	2
46	− 2509.30	− 5186.37	1	102	− 3556.73	1120.40	2	158	3722.73	4854.00	2
47	− 2143.59	− 5401.03	1	103	− 3615.01	941.02	2	159	2597.00	3846.50	2
48	− 1701.97	− 5567.30	1	104	− 4965.56	899.10	2	160	2383.31	3969.31	2
49	− 1365.45	− 5838.66	1	105	− 5122.78	885.34	2	161	2484.19	4520.51	2
50	− 1297.13	− 3768.08	1	106	− 3553.75	171.67	2	162	2805.07	4852.63	2
51	− 994.06	− 4053.32	1	107	− 5194.53	− 278.64	2	163	2116.53	3737.97	2
52	− 737.94	− 4554.44	1	108	− 4223.51	− 599.60	2	164	2637.07	5139.71	2
53	147.76	− 3344.41	1	109	− 2059.83	− 1518.15	2	165	634.82	3635.36	2
54	1662.26	3569.96	1	110	− 3883.63	− 2274.38	2	166	543.62	4228.48	2
55	1139.34	− 3052.97	1	111	− 1803.24	− 1877.30	2				
56	1306.98	− 3703.06	1	112	− 2522.84	− 2304.49	2				

that the limits given above are valid in case of planets with a low absorption due to the disc. Example of companions observed with SPHERE that are embedded in the disc and, for this reason, are very reddened or almost totally extincted are e.g. the debated companions of HD 100546 (Sissa et al. 2018) or the stellar companion R CrA B (Mesa et al. 2019). There is a paucity of studies that quantify the effect of discs on embedded planets, so that it is not possible in this work to draw conclusions on this particular case. In addition,

we have to consider that, due to the fact that the HD 163296 disc is still extremely gas rich, planetary objects embedded into it would be probably surrounded by a circum-planetary disc (CPD) like recently proposed by Christiaens et al. (2019) for the case of PDS 70 b. As demonstrated by Zhu (2015) the flux at NIR wavelengths should be dominated by the disc but recently Szulágyi et al. (2019) concluded, based on the SED, that the best contrast between the circumstellar disc and the CPD is for submillimetre/radio wavelengths, while the CPD observation should be strongly hampered at NIR wavelengths.

Mass limits of a few M_{Jup} are however not enough to give any conclusion about the presence (or not) of the planetary companions proposed by Liu et al. (2018) and Teague et al. (2018). On the other hand, the companion at large separation proposed by Pinte et al. (2018) is just below the detection limit obtained through IRDIS. We were however not able to retrieve it in our data so that further observations and analysis are mandatory to fully exclude or confirm its existence. Finally, the mass limits that we obtain for this star should allow to detect a planet of 6 M_{Jup} at a projected separation of 0.49 arcsec as proposed by Guidi et al. (2018) both with IRDIS and with IFS. The fact that we are not able to recover this planet should rule out its presence confirming what recently found by Rich et al. (2019) with observations in the *J*, *H*, and *K* spectral bands at the Subaru Telescope. However, we have to remember that this planet has been discovered by observations in the *L*' band. As stressed above, due to the disc environment in which it would reside a putative planet would then experience a strong absorption. This could induce a very red spectrum that would make difficult to image it at the shortest wavelengths used for SPHERE. Another possible explanation could be that this object has a very dusty and cool atmosphere. This latter case would be very similar to those of HD 95086 discovered in *L*' band with NACO by Rameau et al. (2013). This planet was then recovered with difficulty with SPHERE using IRDIS in the *K* band and only marginally in *H* band with IFS combining data sets from different epochs (Chauvin et al. 2018). This planet could then be a similar, or even more extreme, case.

In conclusion, our work demonstrates that SPHERE operating in high-contrast imaging mode is able to reach very deep contrast limits for young stellar systems even if it is operating in not ideal conditions. While it was not possible to give any conclusion for the lower mass companions proposed in previous works on this system, we were able to exclude, or at least to put strong constraints on their physical characteristics. Finally, our data seem to exclude the presence, even if with some caveat, of the only candidate companion until now proposed through high-contrast imaging methods.

High-contrast imaging instruments like SPHERE or GPI are providing state-of-art data, whose quality cannot be overcome at present. Given that their limit are not enough to draw a definitive conclusion on the presence of the proposed companions, we then conclude that the difficulties in confirming for this and for similar stars that the observed disc structures are due to the interaction with substellar objects are mainly due to technological limits. We will then need observations with future instrumentations to be able to confirm or to reject the hypothesis of planet/disc interaction to explain these structures.

REFERENCES

Allard F., Hauschildt P. H., Alexander D. R., Tamanai A., Schweitzer A., 2001, ApJ, 556, 357
Allard F., Guillot T., Ludwig H.-G., Hauschildt P. H., Schweitzer A., Alexander D. R., Ferguson J. W., 2003, in Martín E., ed., Proc. IAU Symp. 211, Brown Dwarfs. Astron. Soc. Pac., San Francisco, p. 325
ALMA Partnership et al., 2015, ApJ, 808, L3

Amara A., Quanz S. P., Akeret J., 2015, Astron. Comput., 10, 107
Andrews S. M. et al., 2016, ApJ, 820, L40
Andrews S. M. et al., 2018, ApJ, 869, L41
Ansdell M. et al., 2018, ApJ, 859, 21
Béthune W., Lesur G., Ferreira J., 2017, A&A, 600, A75
Beuzit J.-L. et al., 2019, preprint (arXiv:1902.04080)
Bressan A., Marigo P., Girardi L., Salasnich B., Dal Cero C., Rubele S., Nanni A., 2012, MNRAS, 427, 127
Bryden G., Chen X., Lin D. N. C., Nelson R. P., Papaloizou J. C. B., 1999, ApJ, 514, 344
Chauvin G. et al., 2017, in Reylé C., Di Matteo P., Herpin F., Lagadec E., Lançon A., Meliani Z., Royer F., eds, SF2A-2017: Proceedings of the Annual meeting of the French Society of Astronomy and Astrophysics SHINE, The SpHere INfrared survey for Exoplanets. p. 331
Chauvin G. et al., 2018, A&A, 617, A76
Chen C. H., Pecaut M., Mamajek E. E., Su K. Y. L., Bitner M., 2012, ApJ, 756, 133
Christiaens V., Cantalloube F., Casassus S., Price D. J., Absil O., Pinte C., Girard J., Montesinos M., 2019, preprint (arXiv:1905.06370)
Claudi R. U. et al., 2008, in Reylé C., Di Matteo P., Herpin F., Lagadec E., Lançon A., Meliani Z., Royer F., eds, Proc. SPIE Conf. Ser. Vol. 7014, SPHERE IFS: the Spectro Differential Imager of the VLT for Exoplanets Search. SPIE, Bellingham
Cutri R. M. et al., 2003, VizieR Online Data Catalog, II/246
Delorme P. et al., 2017, in Reylé C., Di Matteo P., Herpin F., Lagadec E., Lançon A., Meliani Z., Royer F., eds, SF2A-2017: Proceedings of the Annual Meeting of the French Society of Astronomy and Astrophysics The SPHERE Data Center: A Reference for High Contrast Imaging Processing. p. 347
Dohlen K. et al., 2008, in McLean I. S., Casali M. M., eds, Proc. SPIE Conf. Ser. Vol. 7014, The Infra-red Dual Imaging and Spectrograph for SPHERE: Design and Performance. SPIE, Bellingham, p. 70143L
Dong R., Li S., Chiang E., Li H., 2018, ApJ, 866, 110
Fedele D. et al., 2018, A&A, 610, A24
Flasseur O., Denis L., Thiébaut É., Langlois M., 2018, A&A, 618, A138
Gaia Collaboration et al., 2018, A&A, 616, A1
Galicher R. et al., 2018, A&A, 615, A92
Garufi A., Quanz S. P., Schmid H. M., Avenhaus H., Buenzli E., Wolf S., 2014, A&A, 568, A40
Garufi A. et al., 2017, A&A, 603, A21
Garufi A. et al., 2018, A&A, 620, A94
Gibbs A., Wagner K., Apai D., Moór A., Currie T., Bonnefoy M., Langlois M., Lisse C., 2019, AJ, 157, 39
Grady C. A. et al., 2000, ApJ, 544, 895
Groff T. D. et al., 2015, Proc. SPIE, 9605, 96051C
Guidi G. et al., 2018, MNRAS, 479, 1505
Huang J. et al., 2018, ApJ, 869, L43
Isella A., Testi L., Natta A., Neri R., Wilner D., Qi C., 2007, A&A, 469, 213
Isella A. et al., 2016, Phys. Rev. Lett., 117, 251101
Isella A. et al., 2018, ApJ, 869, L49
Jensen-Clem R. et al., 2018, AJ, 155, 19
Jin S., Li S., Isella A., Li H., Ji J., 2016, ApJ, 818, 76
Keppler M. et al., 2018, A&A, 617, A44
Kuchner M., 2012, ZODIPIC: Zodiacal Cloud Image Synthesis, Astrophysics Source Code Library
Langlois M. et al., 2014, Proc. SPIE, 9147, 91471R
Liu S.-F., Jin S., Li S., Isella A., Li H., 2018, ApJ, 857, 87
Loomis R. A., Öberg K. I., Andrews S. M., MacGregor M. A., 2017, ApJ, 840, 23
Macintosh B. et al., 2014, PNAS, 111, 12661
Mannings V., Sargent A. I., 1997, ApJ, 490, 792
Marois C., Lafrenière D., Doyon R., Macintosh B., Nadeau D., 2006, ApJ, 641, 556
Marshall J. P. et al., 2014, A&A, 565, A15
Mawet D. et al., 2014, ApJ, 792, 97
Mawet D. et al., 2017, AJ, 153, 44

Mesa D. et al., 2015, A&A, 576, A121
Mesa D. et al., 2019, A&A, 624, A4
Monnier J. D. et al., 2017, ApJ, 838, 20
Montesinos B., Eiroa C., Mora A., Merín B., 2009, A&A, 495, 901
Mora A. et al., 2001, A&A, 378, 116
Müller A. et al., 2018, A&A, 617, L2
Muro-Arena G. A. et al.., 2018, A&A, 614, A24
Pavlov A., Möller-Nilsson O., Feldt M., Henning T., Beuzit J.-L., Mouillet D., 2008, in Proc. SPIE Conf. Ser. Vol. 7019, Advanced Software and Control for Astronomy II. SPIE, Bellingham, p. 701939
Pinilla P. et al., 2018, ApJ, 859, 32
Pinte C. et al., 2018, ApJ, 860, L13
Racine R., Walker G. A. H., Nadeau D., Doyon R., Marois C. 1999, PASP, 111, 587
Rameau J. et al., 2013, ApJ, 772, L15
Rich E. A. et al., 2019, ApJ, 875, 38
Ruane G. et al., 2017, AJ, 154, 73
Setterholm B. R. et al., 2018, ApJ, 869, 164
Sissa E. et al., 2018, A&A, 619, A160
Sitko M. L., Grady C. A., Lynch D. K., Russell R. W., Hanner M. S., 1999, ApJ, 510, 408
Soummer R., Pueyo L., Larkin J., 2012, ApJ, 755, L28
Szulágyi J.et al., 2019, MNRAS, 487, 1248
Takahashi S. Z., Inutsuka S.-i., 2014, ApJ, 794, 55
Teague R., Bae J., Bergin E. A., Birnstiel T., Foreman-Mackey D., 2018, ApJ, 860, L12
Tilling I. et al., 2012, A&A, 538, A20
van den Ancker M. E., The P. S., Tjin A Djie H. R. E., Catala C., de Winter D., Blondel P. F. C., Waters L. B. F. M., 1997, A&A, 324, L33
van den Ancker M. E., de Winter D., Tjin A Djie H. R. E., 1998, A&A, 330, 145
van der Marel N., Williams J. P., Bruderer S., 2018, ApJ, 867, L14
Vigan A., Moutou C., Langlois M., Allard F., Boccaletti A., Carbillet M., Mouillet D., Smith I., 2010, MNRAS, 407, 71
Zhang K., Blake G. A., Bergin E. A., 2015, ApJ, 806, L7
Zhu Z., 2015, ApJ, 799, 16
Zurlo A. et al., 2014, A&A, 572, A85
Zurlo A. et al., 2016, A&A, 587, A57

[1]*INAF-Osservatorio Astronomico di Padova, Vicolo dell'Osservatorio 5, Padova, I-35122, Italy*
[2]*INCT, Universidad De Atacama, calle Copayapu 485, Copiapó, Atacama, Chile*
[3]*Univ. Lyon, Univ. Lyon 1, ENS de Lyon, CNRS, CRAL UMR 5574, F-69230 Saint-Genis-Laval, France*
[4]*Aix Marseille Univ., CNRS, CNES, LAM, Marseille, France*
[5]*INAF – Osservatorio Astrofisico di Arcetri, Largo Enrico Fermi 5, I-50125 Firenze, Italy*
[6]*Institut d'Optique Graduate School, Université de Lyon, UJM-Saint-Etienne, CNRS, Laboratoire Hubert Curien UMR 5516, F-42023, Saint-Etienne, France*
[7]*Unidad Mixta Internacional Franco-Chilena de Astronoma (CNRS, UMI 3386), Departamento de Astronomía, Universidad de Chile, Camino El Observatorio 1515, Las Condes, Santiago, Chile*
[8]*Univ. Grenoble Alpes, CNRS, IPAG, F-38000 Grenoble, France*
[9]*Max-Planck-Institut für Astronomie, Königstuhl 17, D-69117 Heidelberg, Germany*
[10]*INAF – Osservatorio Astronomico di Brera, Via E. Bianchi 46, I-23807 Merate, Italy*
[11]*Nucleo de Astronomia, Facultad de Ingenieria y Ciencias, Universidad Diego Portales, Av. Ejercito 441, Santiago, Chile*
[12]*Escuela de Ingenieria Industrial, Facultad de Ingenieria y Ciencias, Universidad Diego Portales, Av. Ejercito 441, Santiago, Chile*
[13]*LESIA, Observatoire de Paris, Université PSL, CNRS, Sorbonne Université, Univ. Paris Diderot, Sorbonne Paris Cité, 5 place Jules Janssen, F-92195 Meudon, France*
[14]*Geneva Observatory, University of Geneva, Chemin des Maillettes 51, CH-1290 Versoix, Switzerland*

[15]*INAF – Osservatorio Astronomico di Capodimonte, Salita Moiariello 16, I-80131 Napoli, Italy*
[16]*DOTA, ONERA, Université Paris Saclay, F-91123 Palaiseau, France*
[17]*Institute for Particle Physics and Astrophysics, ETH Zurich, Wolfgang-Pauli-Strasse 27, CH-8093 Zurich, Switzerland*
[18]*STAR Institute, Université de Liége, Allée du Six Août 19c, B-4000, Liége, Belgium*

[19]*Department of Astronomy, University of Michigan, 1085 S. University Ave., Ann Arbor, MI 48109-1107, USA*
[20]*Hamburger Sternwarte, Gojenbergsweg 112, D-21029 Hamburg, Germany*

This paper has been typeset from a TEX/LATEX file prepared by the author.